Available online at www.sciencedirect.com
ScienceDirect
Signal Processing 87 (2007) 3202–3217
SIGNAL PROCESSING
www.elsevier.com/locate/sigpro

Some uncertain factor analysis and improvement in spaceborne synthetic aperture radar imaging

Shi-qi Huang*, Dai-zhi Liu

Sec. 602, Xi'an Research Institute of Hi-Tech, Hongqing Town, 710025 Xi'an, PR China

Received 14 March 2007; received in revised form 20 June 2007; accepted 3 July 2007
Available online 10 July 2007

Abstract

Synthetic aperture radar (SAR) is an active microwave remote sensing imaging radar, which can obtain abundant electromagnetic information from ground objects, especially in some regions where optics and infrared remote sensing do not work well. It has been widely applied in civil and military fields. But there are some uncertain factors in SAR imaging which not only affect SAR imaging, but also obstruct interpretation and applications of SAR images. In order to restrain and improve these uncertain factors, this paper deeply analyzes and discusses the uncertainties of spaceborne SAR imaging system from the SAR imaging mechanism and imaging process, and proposes some corresponding improved algorithms. These uncertainties, which are caused by Doppler parameter estimation, range migration, speckle noise and object azimuth angle, are explained in detail. The raw data of ERS-2 are used to test these methods, and the experimental results prove that it is efficient for them to improve and control the uncertain factors, and there will be some referential value for further studying SAR imaging and applications.

Keywords: Spaceborne SAR imaging; Uncertain factor; Doppler parameter estimation; Range migration; Speckle noise; Aspect angle

1. Introduction

Synthetic aperture radar (SAR) is capable of acquiring data in all weather conditions and is not affected by cloud cover or different sunlight conditions. And it can provide a great deal of useful remote sensing information via different frequency and different polarization images. At present, SAR has become one of the most powerful and efficient tools in investigating and monitoring earth's environment, such as land-cover mapping, flood monitoring, polar ice investigation, agriculture assessment and ocean monitoring.

Since SAR imaging technique was born in 1950s, it has made great progress. SAR develops gradually from single wave band, single polarization, fixed incidence angle and single imaging model to multiple wave bands, multiple polarization, variable incidence angle and multiple imaging models. Currently the research issue of SAR imaging is high-resolution imaging algorithm and real-time imaging model, and in addition the applying issue is how to extract useful information from SAR images as fast as possible. Both SAR imaging and SAR application are not only a progressive development process but also a continual perfection

*Corresponding author. Tel.: +86 29 83348183.
E-mail address: huang_shi_qi@163.com (S.-q. Huang).

0165-1684/$ - see front matter © 2007 Elsevier B.V. All rights reserved.
doi:10.1016/j.sigpro.2007.07.001

process. Although some delightful achievements have been gained, the resolution does not reach its physical utmost or the optics remote sensing resolution level. Secondly, whether in theory or engineering, there are many deficiencies, for instance, high-resolution imaging algorithm, motion migration compensation methods and efficient speckle noise filters.

SAR is a quite important microwave imaging remote sensing technique and has already turned into an indispensable detection instrument for the earth observation system. With the development of high-resolution SAR imaging, the applied fields of SAR will be more widened. At the same time, the SAR image quality is also improved continually and they provide more object information. However, not only in the high-resolution SAR images but also in the low-resolution images, the uncertain factors universally exist, which brings serious influence for SAR image applications. Therefore, many literates have done a great number of researches and gained many achievements in this aspect in recent years [1–6]. But these results are mostly based on the stochastic analysis theory, considering the random uncertainty. In addition, some results consider that the uncertainty of remote sensing is from the sensor system parameters. This article analyzes in detail the uncertain factors, which exist in spaceborne SAR imaging, from SAR imaging principle and SAR image processing process and discusses the influence that uncertain factors bring for SAR imaging quality and SAR image interpretation. What's more, some novel methods or algorithms for controlling or improving the uncertain factors are proposed. The raw data of ERS-2 is used to test the effectiveness and the validity of these methods. The experimental results represent that they are efficient and right, and in some ways they can improve the uncertainties. In the same way, these methods or strategies may be used to improve the uncertainty of airborne SAR imaging.

In Section 2 the influence of the inaccurate estimation of Doppler parameters on spaceborne SAR imaging is analyzed, and the novel mean frequency shift correlation (MFSC) algorithm is proposed. Section 3 explains the uncertainty that range migration brings for SAR imaging. In Section 4 the impact caused by speckle noise for SAR image application is discussed. In order to restrain speckle noise, some new methods are addressed. Section 5 describes the uncertainty which object azimuth angle brings for the interpretation and judgment of SAR images. Finally, some conclusions are presented in Section 6.

2. Uncertainty of Doppler parameter estimation

The aim of SAR imaging processing is to obtain the two-dimension distribution function of object region scattering coefficients, which are two-dimension correlation process. Usually, it is divided into two parts, which includes range compression phase and azimuth compression phase. Range compression is one-dimension invariant shift course, which is quite easy. However, azimuth compression is much more difficult than range compression because there is a range migration phenomena, and it is two-dimension shift variant correlated course. In fact, how to solve the shift variant problem of azimuth compression is the key for the SAR imaging algorithm. The different processing methods of the shift variants lead to the different imaging algorithms. For example, there are many typical imaging algorithms, such as Range-Doppler (RD) algorithm [7], wave-number domain algorithm [8] and chirp-scaling (CS) algorithm [9]. Where, RD algorithm is a relatively mature method, whose range compression and azimuth compression is processed, separately. The key part of RD algorithm is Doppler parameter estimation, for azimuth reference function is the expression of Doppler parameters. If the estimation of Doppler centroid frequency f_{DC} is imprecise, the signal to noise rate (SNR) of image will drop, and the azimuth blurring will increase, which will make object position motion; if the estimation of Doppler frequency rate f_{DR} is imprecise, the images will defocus and pixel resolution will drop. At present, side-looking imaging model is still a main way, and it usually employs RD algorithm. The most important part of RD algorithm is Doppler frequency rate estimation. Therefore, the next work is to discuss Doppler frequency rate estimation problem.

2.1. Doppler parameters description

The key technique of azimuth compression or azimuth focusing is Doppler parameter estimation, which includes Doppler centroid frequency f_{DC} and Doppler frequency rate f_{DR}. They compose the azimuth-matching filter in azimuth time domain or frequency domain. Suppose that the radar sends a frequency-modulated chirp pulse signal $s(t)$. After it

is received and compressed in range, it is

$$g_n(t) = \exp\left(\frac{-\mathrm{j}4\pi R_n}{\lambda}\right) \mathrm{sinc}\,(u), \tag{1}$$

where n is the nth pulse, $u = \pi k \tau_p (t - 2R_n/c)$, and k is chirp slope, τ_p is pulse duration (pulse width). When the maximum value of $|g_n(t)|$ appears, the time is $t_n = 2R_n/c$. Here, the value of $|g_n(t)|$ is

$$g_n(t_n) = \exp\left(\frac{-\mathrm{j}4\pi R_n}{\lambda}\right). \tag{2}$$

All pulses repeat the course in the observation time. In fact, it is a sampling series in slow time field:

$$g_n(s|x_c, R_c) = \exp\left[\frac{-\mathrm{j}4\pi R(s)}{\lambda}\right], \tag{3}$$

where $R_n = R(s_n)$. The geometry of the strip-mode acquisition of spaceborne SAR is shown in Fig. 1 [10,11].

In Fig. 1, s is slow time along the satellite track, x is ground-track position, V is ground track velocity, s_0 is time when the target is in the center of the radar illumination pattern, H is spacecraft height, R_g is ground range, $R(s)$ is the range from spacecraft to target, and R_0 is the minimum range from the spacecraft to the target. Here, R_0 is given by

$$R_0 = \sqrt{H^2 + R_g^2} = R_{\mathrm{near}} + n \times \frac{c}{F_s}, \tag{4}$$

where c is the velocity of light, F_s is range sampling rate and n is the number of sampling point, namely, the number of range gate.

The complex phase of the return echo may be gained from Eq. (3), and it is given by

$$C(s) = \exp\left[-\mathrm{i}\frac{4\pi}{\lambda} R(s)\right], \tag{5}$$

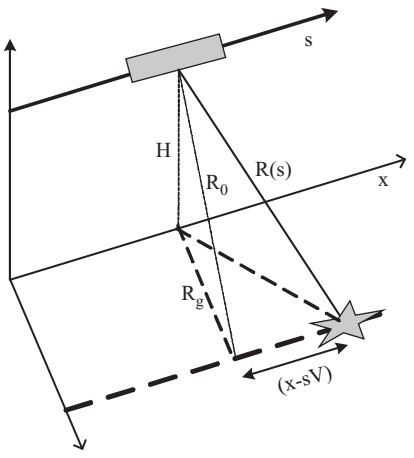

Fig. 1. Geometry of strip map spaceborne SAR.

where the range is

$$R^2(s) = H^2 + R_g^2 + (x - sV)^2. \tag{6}$$

This is a hyperbola that we can approximate using a parabola, which spreads near $s_0 = x_0/V$,

$$R(s) = R_0 + \dot{R}_0(s - s_0) + \frac{\ddot{R}_0}{2}(s - s_0)^2 + \cdots, \tag{7}$$

where, the dot indicates derivative with respect to slow time s. Now we need to calculate $\dot{R}$ and $\ddot{R}$ in terms of spacecraft parameters. Let us start with $\dot{R}$ by taking the derivative of R^2 with respect to s.

$$\frac{\partial R^2}{\partial s} = 2R\dot{R} \Rightarrow \dot{R} = \frac{1}{2R}\frac{\partial R^2}{\partial s}. \tag{8}$$

We note that $\dot{R}_0$ is the velocity of the spacecraft in the range direction at the time s_0 and thus a measurement of the Doppler shift when the target is in the center of the radar illumination pattern:

$$\dot{R}_0 = -V\frac{(x - s_0 V)}{R_0}. \tag{9}$$

The range acceleration $\ddot{R}$ is the derivative of the range rate $\dot{R}$:

$$\begin{aligned}\ddot{R} &= \frac{\partial}{\partial s}\left(\frac{1}{2R}\frac{\partial R^2}{\partial s}\right) \\ &= \frac{1}{2}\left[\frac{1}{R}\left(\frac{\partial^2 R^2}{\partial s^2}\right) + \frac{-1}{R^2}\left(\frac{\partial R}{\partial s}\right)\left(\frac{\partial R^2}{\partial s}\right)\right].\end{aligned} \tag{10}$$

This can be written as

$$\ddot{R} = \frac{V^2}{R} + \frac{-V^2(x - sV)^2}{R^3} = \frac{V^2}{R}\left[1 - \frac{(x - sV)^2}{R^2}\right]. \tag{11}$$

For the orbital characteristics of the spacecraft, the second term is small so we have $\ddot{R}_0 \cong V^2/R_0$. Now we can write the phase of the return signal as a function of geometry and speed

$$C(s) = \exp\left\{-\mathrm{i}\frac{4\pi}{\lambda}\left[R_0^2 + \dot{R}_0(s - s_0) + \frac{\ddot{R}_0}{2}(s - s_0)^2\right]\right\} \tag{12}$$

or

$$\begin{aligned}C(s) = {} & \exp\left\{\mathrm{i}\frac{4\pi R_0^2}{\lambda}\right\} \\ & \times \exp\left\{\mathrm{i}2\pi\left[\frac{-2V}{\lambda}\frac{(x - s_0 V)}{R_0}(s - s_0)\right.\right. \\ & \left.\left. + \frac{-2V^2}{\lambda R_0}\frac{(s - s_0)^2}{2}\right]\right\}.\end{aligned} \tag{13}$$

This function is another frequency-modulated chirp where we can get the two important parameters: the Doppler centroid frequency and Doppler frequency rate. They are given by

$$f_{DC} = -\frac{2V}{\lambda}\frac{(x - s_0 V)}{R_0}, \tag{14}$$

$$f_{DR} = -\frac{2V^2}{\lambda R_0}. \tag{15}$$

We note that Doppler frequency rate is computed by the ground track velocity of satellite V, wavelength λ and range from target to spacecraft track R_0.

2.2. MFSC algorithm

R-D algorithm is a typical SAR imaging algorithm, which makes range compression and azimuth compression, respectively. In azimuth compression, the azimuth reference function in frequency domain is given by

$$H_a(f_a) = \exp\left(j\pi\frac{f_a^2}{f_{DR}}\right)\exp\left(j2\pi\frac{f_{DC}}{f_{DR}}f_a\right), \tag{16}$$

where, f_a is azimuth frequency, f_{DC} is Doppler centroid frequency, and f_{DR} is Doppler frequency rate.

From Eq. (16), we may see that the Doppler parameters are very important for SAR imaging. Because they are the parameters of the azimuth-matching filter, furthermore, the precision of Doppler parameter estimation directly impacts the quality of SAR imaging. Therefore, since the day when SAR came into being, the Doppler parameter estimation has been being the hotspot and difficulty, for it is relative with the azimuth focus. The early Doppler parameter was estimated by ephemeris data and attitude data. The ephemeris data is relative stabilization, while the attitude data has some errors, thus, the accuracy of Doppler parameter estimation is determined by the accuracy of measurement of satellite attitude data and the estimated precision of orbit parameter based on the track data. The measurement accuracy of attitude data is confined by the instrument precision, and the smoothing and revision of track data require some delay. Therefore, there are some difficulties for Doppler parameter to satisfy the imaging requirement with ephemeris data and attitude data. The most important thing is that the estimated precision is low and the defocusing effect is serious, which causes an blurry image.

In order to satisfy practical demand many methods are developed to estimate Doppler parameter from the echo data. Some methods have higher estimated precision, so they are usually employed. There are a few familiar Doppler centroid frequency estimation algorithms, such as energy equalization method [12], image field method [13], related functions method and sign correlation method [14]. In the same way, the familiar Doppler frequency rate estimation algorithms include sub-aperture correlation method (called map drift algorithm, MD) [14–16], time-frequency analysis method [17], image contrast method [18] and minimum entropy method [19]. The common disadvantage of these algorithms is that the computational operation is relatively complex, the computation is great and they can not be employed to realize the real-time imaging. Subsequently, some literates estimate the Doppler frequency rate through the return echo data, such as reflectivity displacement method (RDM) [20] and shift-and-correlation (SAC) method [21]. However, the two methods are both fit for airborne SAR imaging system and are not directly used for spaceborne SAR system.

The estimated value only infinitely approaches the true value. Now there are no perfect estimation methods, and each method has its limitation. In other words, every way has its uncertainty. For example, the energy equalization method and the correlation Doppler centroid estimation method are fit for the symmetrical background condition; image field method demands that the Doppler frequency rate is known and accurate, and that the probable scope of centroid frequency is known. MD algorithm and image contrast method adapt to the non-symmetrical region, especially, having strong reflective objects, the results are relatively precise.

For side-looking imaging radar, the influence brought by Doppler frequency rate is larger than Doppler centroid frequency. In order to obtain high quality SAR images, we propose a novel Doppler frequency rate estimation method, which is called MFSC algorithm. MFSC algorithm directly estimates Doppler frequency rate from the return echo data, without iteration, reducing the calculated scale and saving the processed time. The block diagram of the MFSC algorithm is shown in Fig. 2. Because Doppler frequency rate is not a constant, and it always changes with the range change between radar and object, as is shown in Fig. 3, the MFSC algorithm is made up of two parts. One is the center frequency rate (mean frequency rate) and the other is the adjustable frequency rate. Firstly, compute each gate Doppler frequency rate, then sum and mean, which acts as

center frequency rate. Secondly, make frequency shift correlation operation in frequency domain, and acquire the peak value, whose position is the adjustable value of Doppler frequency rate. Finally, that the basic center value adds corresponding adjustable value of each gate is the Doppler frequency rate estimated value of each gate.

In MFSC algorithm, the center frequency rate is computed with Eq. (15), and the SAC algorithm is used to compute the adjustable frequency rate. If the SAC algorithm is directly utilized to process spaceborne SAR echo data, the result is not ideal and the image can not be obtained, as is shown in Fig. 5(a)(A)–(d)(A), because the method aims at airborne SAR.

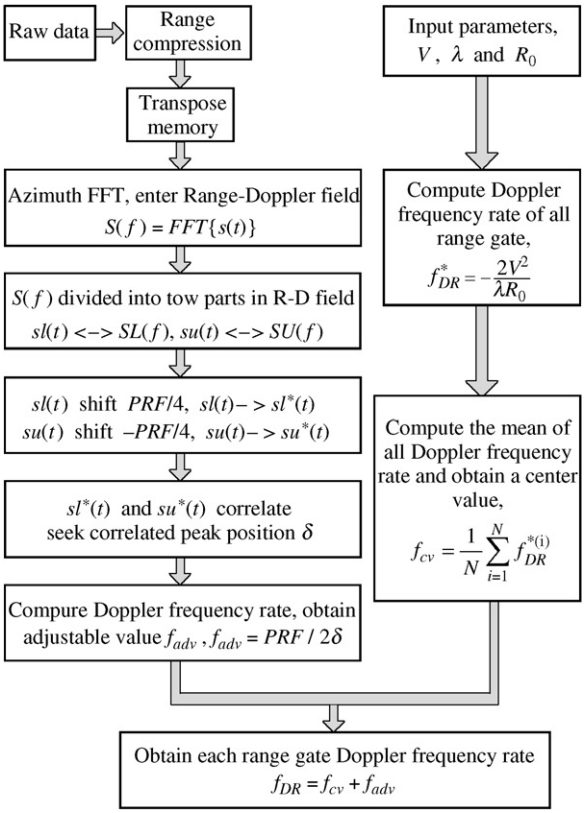

Fig. 2. The block diagram of MFSC algorithm.

Assume that the echo signal of a point object is

$$s(t) = \exp\left[i\pi f_{DR}(t - t_0)^2\right] \quad t_0 - T/2 \leqslant t \leqslant t_0 + T/2. \tag{17}$$

Signal $s(t)$ is divided into two parts in frequency domain, which are SL(f) and SU(f), denoting the lower half and the upper half of Doppler spectrum, respectively. SAC algorithm refers to the relative frequency shift of SL and SU, then makes correlation. The principle of SAC is shown in Fig. 4.

Because $s(t)$ has the feature of large time-frequency product, the corresponding time domain signal of SL(f) and SU(f) is sl(t) and su(t), respectively. They are given by

$$\begin{cases} \mathrm{sl}(t) = \exp\left[i\pi f_{DR}(t - t_0)^2\right], & t_0 - T/2 \leqslant t \leqslant t_0, \\ \mathrm{su}(t) = \exp\left[i\pi f_{DR}(t - t_0)^2\right], & t_0 \leqslant t \leqslant t_0 + T/2. \end{cases} \tag{18}$$

Then, sl(t) and su(t) make frequency shift processing, SL(f) shifts PRF/4 to upper half of the spectrum and SU(f) shifts PRF/4 to lower half of the spectrum, where PRF is pulse repetition frequency. The results are given by

$$\begin{cases} \mathrm{SL}^+(f) = \mathrm{SL}(f - \mathrm{PRF}/4), \\ \mathrm{SU}^+(f) = \mathrm{SU}(f + \mathrm{PRF}/4). \end{cases} \tag{19}$$

The corresponding time domain signals are $\mathrm{sl}^+(t)$ and $\mathrm{su}^+(t)$, respectively, and they are given by

$$\mathrm{sl}^+(t) = \mathrm{sl}(t)\exp\left(i2\pi\frac{\mathrm{PRF}}{4}t\right) = \exp\left[-i\pi f_{DR}\left(\frac{\delta}{2}\right)^2 + i\pi f_{DR} t_0 \delta\right]$$

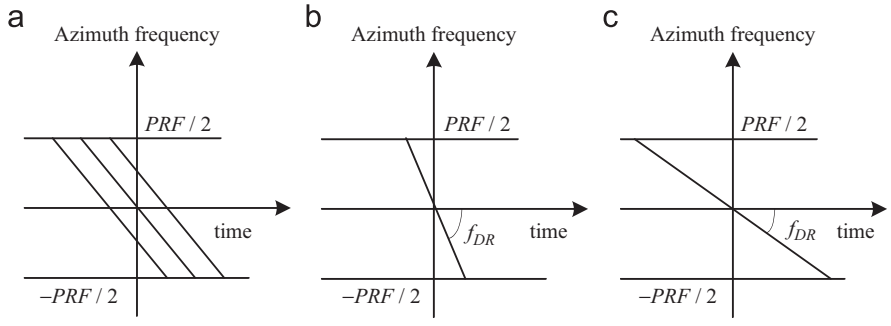

Fig. 3. The changes of Doppler frequency rate with range. (a) Doppler rate; (b) near range; and (c) far range.

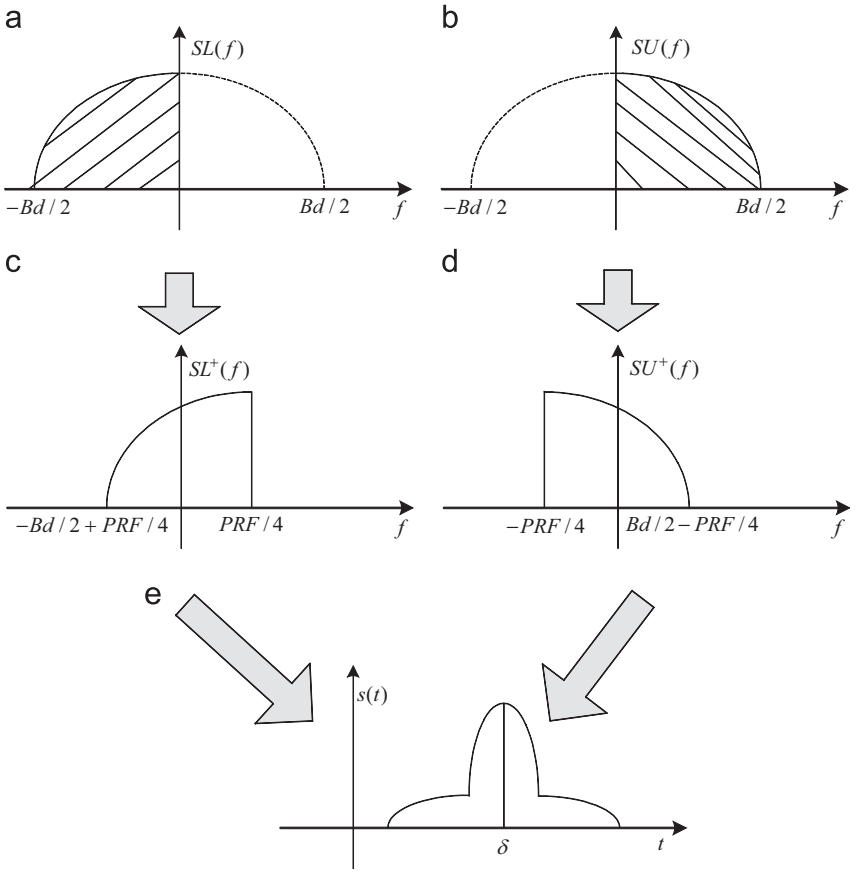

Fig. 4. Sketch diagrams of shift and correlation. (a) Lower half spectrum; (b) upper half spectrum; (c) lower half spectrum after shift; (d) upper half spectrum after shift; and (e) correlation result.

$$\times \exp\left[\mathrm{i}\pi f_{\mathrm{DR}}\left(t - t_0 + \frac{\delta}{2}\right)^2\right], \quad \left[t_0 - \frac{T}{2} \leqslant t \leqslant t_0,\right] \tag{20}$$

$$\begin{aligned} \mathrm{su}^+(t) &= \mathrm{su}(t)\exp\left(-\mathrm{i}2\pi\frac{\mathrm{PRF}}{4}t\right) \\ &= \exp\left[-\mathrm{i}\pi f_{\mathrm{DR}}\left(\frac{\delta}{2}\right)^2 - \mathrm{i}\pi f_{\mathrm{DR}} t_0 \delta\right] \\ &\quad \times \exp\left[\mathrm{i}\pi f_{\mathrm{DR}}\left(t - t_0 - \frac{\delta}{2}\right)^2\right], \quad \left[t_0 \leqslant t \leqslant t_0 + \frac{T}{2},\right] \end{aligned} \tag{21}$$

where

$$\delta = \frac{\mathrm{PRF}}{2f_{\mathrm{DR}}}. \tag{22}$$

If $\mathrm{sl}^+(t)$ and $\mathrm{su}^+(t)$ correlate, the correlation peak position will appear in δ which is shown in Fig. 4(e). Assume that the position δ of correlation peak and pulse repeat frequency PRF are given, f_{DR} may be gained by Eq. (22), as is called the SAC method. It is a pity that the SAC method is only used by the airborne SAR and is unfit for low contrast reflected coefficient ground surface.

The MFSC method is an autofocus algorithm that has high-calculated efficiency and some similar sections as the MD algorithm. But the MD algorithm makes azimuth correlation with the corresponding images of lower half and upper half of azimuth spectrum so that it can obtain Doppler frequency rate errors. MD algorithm is an autofocus algorithm based on image field, and its computation burden is great, what's more, it needs reiterative operation to form an image. Therefore, it is not fit for real-time imaging processing. However, the MFSC algorithm does not need reiterative operation, which may greatly reduce calculated

scale. At the same time, it may reach better precision for Doppler frequency rate estimation value, and it is not only fit for real-time imaging processing but also agrees with all kinds of terrain. Experiment data comes from ERS-2, and Fig. 5 shows different terrain imaging results with different Doppler frequency rate estimation algorithm for spaceborne SAR. In Fig. 5, the image (A) is with the SAC algorithm, the image (B) is with the Eq. (15), the image (C) is with the MD algorithm and the image (D) is with the MFSC algorithm. At the same time, the natural scenes of Fig. 5 (a)–(d) are city, mountain, flat and ocean, respectively. The results verify the effectiveness and feasibility of the MFSC algorithm.

3. Uncertainty brought by range migration

In SAR imaging system, the relative movement between radar antenna and target makes that the change of the slant distance exceeds one range resolution cell, and that the echo of the same object falls in different range gate. This phenomenon is called range migration.

It badly influences the SAR image quality and makes SAR image cause uncertainty. So range cell migration correction must be done in SAR imaging, otherwise, it will make radar signal couple in range and azimuth direction, which causes a lot of the matter for SAR image interpretation and target location.

For instance, the ship position takes place range migration phenomenon in Fig. 6. The practical position of the ship should be at point A, but it runs to point B. This is because the range migration curve occurs. Without any reference object, range migration can raise many errors, which will result in it being unable to locate and recognize the targets. Therefore, range migration correction is a very important step in SAR imaging algorithm.

In Fig. 1, the slant distance from point target to radar carrier derives from the geometrical relationship of SAR imaging. And it is given by

$$R(s) = R(s_0) - \frac{\lambda}{2}\left[f_{\mathrm{DC}}(s-s_0) + \frac{1}{2}f_{\mathrm{DR}}(s-s_0)^2\right]. \tag{23}$$

Then the range migration quantity ΔR is

$$\begin{aligned}\Delta R &= R(s) - R(s_0) \\ &= -\frac{\lambda}{2}\left[f_{\mathrm{DC}}(s-s_0) + \frac{1}{2}f_{\mathrm{DR}}(s-s_0)^2\right].\end{aligned} \tag{24}$$

Place $s - s_0 = (f - f_{\mathrm{DC}})/f_{\mathrm{DR}}$ into Eq. (24), then

$$\Delta R = \frac{\lambda}{4f_{\mathrm{DR}}}f_{\mathrm{DC}}^2 - \frac{\lambda}{4f_{\mathrm{DR}}}f^2 = \Delta R_1 + \Delta R_2, \tag{25}$$

where $\Delta R_1 = (\lambda/4f_{\mathrm{DR}})f_{\mathrm{DC}}^2$, $\Delta R_2 = -(\lambda/4f_{\mathrm{DR}})f^2$ and f is azimuth frequency. ΔR_1 is called linear range migration (also called range walk). ΔR_1 is mainly caused by the rotation of the earth. For side-looking airborne SAR, $f_{\mathrm{DC}} = 0$; in spaceborne SAR it may be approximately thought $f_{\mathrm{DC}} = 0$. Therefore, ΔR_1 is equal to 0. ΔR_2 is called range migration curve, which is primarily caused by the difference of slant distance that the target is in the big synthetic aperture, in other words, it is the relative movement between target and radar.

Place $f_{\mathrm{DR}} = -\frac{2V^2}{\lambda R_0}$ into ΔR_2, then

$$\Delta R_2 = \frac{\lambda^2 R_0}{8V^2}f^2. \tag{26}$$

Eq. (26) is discretized towards two directions, and it is written as

$$\Delta R_2 = \frac{\lambda^2}{8V^2}\left(R_0 + \frac{mc}{2f_{\mathrm{s}}}\right)\left(\frac{PRF}{N_{\mathrm{a}}}n\right)^2, \tag{27}$$

where n and m are the azimuth frequency number and range gate order number, respectively. N_{a} is the length of Fourier transform at azimuth direction, PRF is pulse repetition frequency, f_{s} is the sampling frequency of the return echo and c is the velocity of light. Because the range migration is time domain linearity, it can be corrected in time domain, which is simple and convenient. The demand and the process of range migration correction are various for different imaging algorithm. For example, range migration correction can be finished at time domain or frequency domain for the RD algorithm; and it may finish range walk in time domain and finish range curve in frequency. Therefore, many different RD algorithms are formed in terms of range migration correction methods. In general, like RD algorithm and wave-number domain algorithm, using the interpolation way corrects the range migration. The CS algorithm multiplies a linear phase to finish the range migrant correction at range direction in frequency domain. So the CS algorithm avoids abundant interpolation operations and is adapted for squint looking imaging processing, but it is only fit for linear chirp signal. Range migration curve is shown in Fig. 7 [22]. Although range

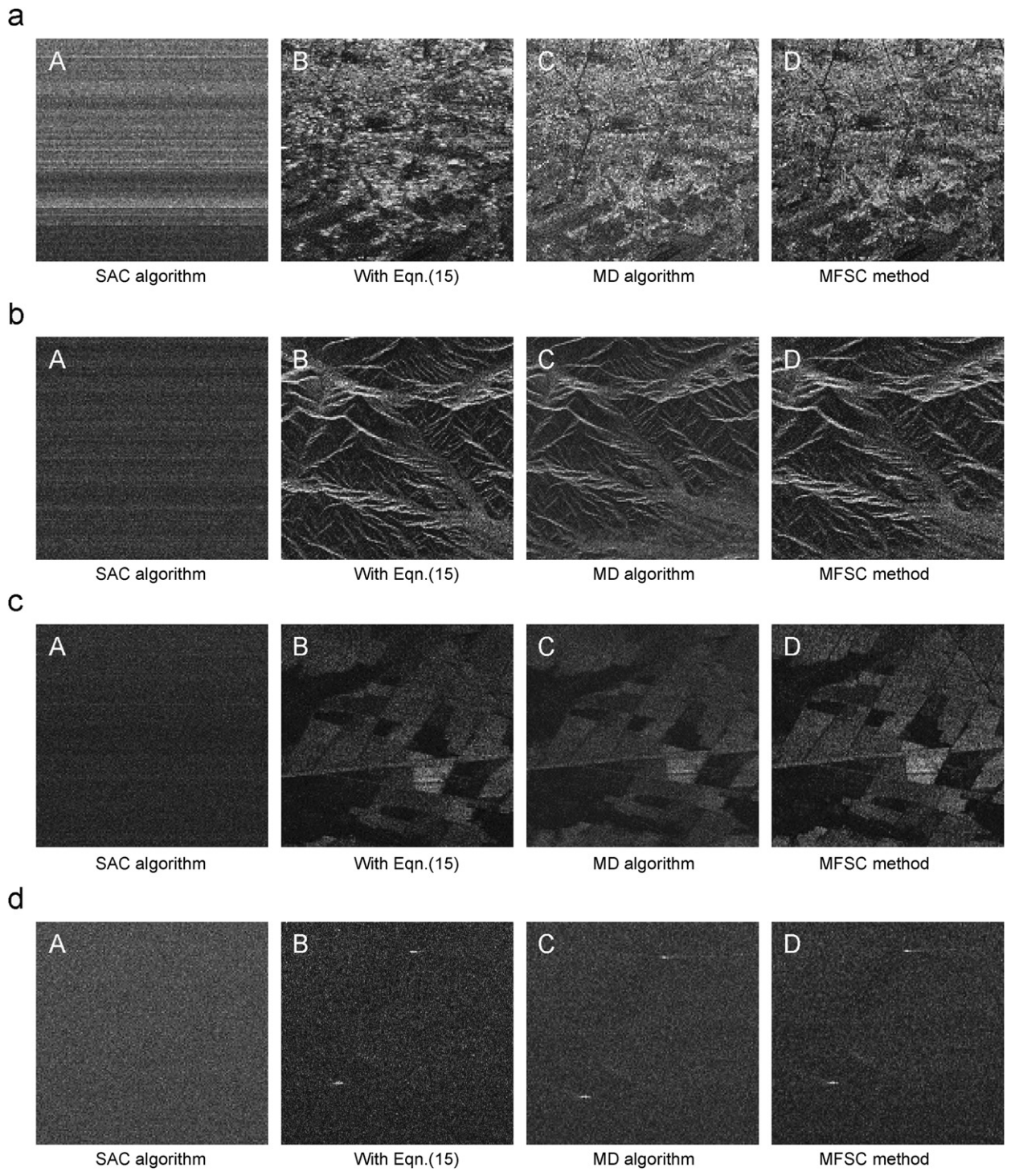

Fig. 5. Imaging results of different Doppler frequency rate estimation for spaceborne SAR. (a) City scene; (b) Mountain scene; (c) Flat scene; and (d) Ocean scene.

migration is a inevitable phenomenon in SAR processing, its scale changes with the different system parameters. The migration compensation is not always needed unless the maximum range migration is greater than the quarter range resolution cell.

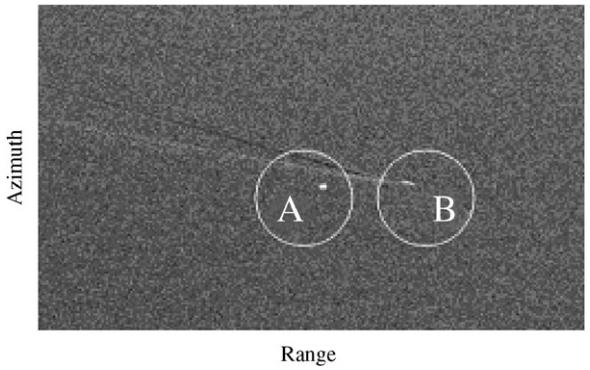

Fig. 6. A SAR image without range migration correction.

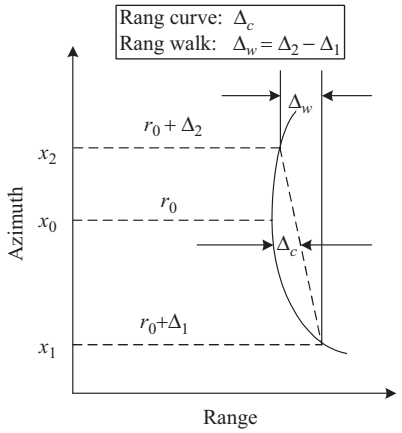

Fig. 7. Range migration curve.

4. Uncertainty caused by speckle noise

A SAR image is a mapping of the scattering characteristic of the ground object to radar wave. The imaging radar transmits an electromagnetic wave that is purely coherent wave. When the electromagnetic wave illuminates an object, the interference actions happen between scatterers on the surface of the object, which causes speckle noise. Except that speckles of SAR image can provide a little of information, most of them are analogous noise and obstruct the application of SAR. The uncertainty caused by speckle noise mostly represents the following aspects

(1) Uncertainty of SAR image interpretation: The existence of speckle noise brings a lot of difficulties for the ground object interpretation, especially, isolated point object and building. They will produce a lot of false alarm rate.

(2) Uncertainty of the SAR image classification: Classification of SAR image target is an important application for SAR. However, the existence of speckle noise makes it very difficult for edge abstraction, image segmentation, target recognition and classification.

(3) Ground surface parametric inversion: Ground surface parametric inversion from SAR image, especially, quantitative reversal development is in need of precise radar image, but the existence of speckle noise makes it difficult to estimate SAR image.

Therefore, smoothing speckle noise is an important post-processing work for SAR imaging. Although speckle noise does not smooth completely, it can be filtered as much as possible. As long as speckle noise is effectively restrained, the uncertainties can improve for SAR image interpretation, SAR image classification and ground surface parametric inversion. This section firstly discusses the mechanism of speckle noise, and then proposes some new methods to smooth speckle noise for SAR image from different aspects.

4.1. Mechanisms and model of speckle noise

A radar resolution cell is made up of a great many of scatterers, which is shown in Fig. 8. Under ideal conditions, the turned echo of these scattering cells is spherical wave. On spherical surface their amplitudes are equivalent everywhere. Because these scatterers come from within a same resolution cell, SAR can not distinguish them. Therefore, there are hundreds and hundreds of scatterers in the earth surface cell where the radar pulse illuminates at every moment. The size of these scatterers is equivalent to the wavelength. The total echo of

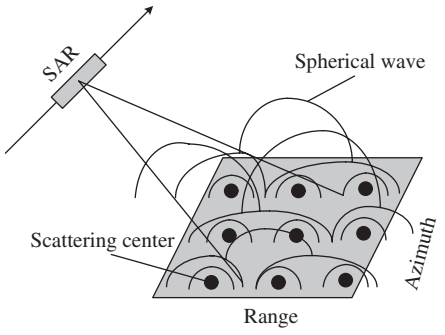

Fig. 8. The principle of speckle noise.

the cell is coherent superposition of each scatterers echo, and the final imaging result of the cell reflects the vector sum of mass scattering echo. The phase of each scatterer echo correlates not only with the distance from them to sensor but also with the characteristic of the scattering material. So it leads to that the intensity of the accepted echo signal is not completely determined by the scattering coefficient of a ground object. Usually, the intensity has great random fluctuation surrounding the value of the scattering coefficient. This phenomenon is called decline. The decline makes that the gray value of the SAR image is not even for the uniformity scattering coefficient area. Therefore, the SAR image has a lot of fluctuant granules, which is called speckle effect [23].

Goodman proposed the concept of complete growth speckle noise, which behaves in uniform region or weak texture region. The model of complete growth speckle noise is generally taken for multiplying model [23], and its expression is given by

$$I(i,j) = R(i,j)F(i,j), \tag{28}$$

where (i,j) is the coordinate of resolution cell center pixel at range and azimuth direction, $I(i,j)$ is the observed image and $R(i,j)$ is the radar scattering characteristic of a random ground object. $F(i,j)$ is the speckle noise which is caused by decline course. Besides, random process $R(i,j)$ and $F(i,j)$ are mutually independent. The speckle noise of some areas is incomplete in growth, such as building area, edge region or texture area. Here, we may employ the speckle noise model that Ubaby founded in 1986 [24]. The definition is given by

$$I(i,j) = \mu T(i,j)F(i,j). \tag{29}$$

where μ is the mean of the image. $T(i,j)$ is texture function value at (i,j), which is a random variable. Through its change, ground scene random fluctuation state can be described. Furthermore, at anyone of the points, $T(i,j) \geqslant 0$ and $\mu_T = E\{T\} = 1$. $F(i,j)$ is the speckle noise which is caused by signal decline, for all (i,j) positions, $F(i,j) \geqslant 0$ and $\mu_F = E\{F\} = 1$. $T(i,j)$ and $F(i,j)$ are mutually independent.

4.2. Smoothing speckle noise with data fusion method

The main difficulty is how to preserve detailed information and good visual effect while reducing speckle noise. The speckle noise reduction techniques are classified into two types, multi-look processing techniques and filter processing techniques. The latter includes space-domain and transform-domain filters. The multi-look smoothing method reduces the space resolution of the image to improve its radiometric resolution. With the development of SAR image applications, multi-look processing techniques can not satisfy many of the practical requirements, and space-domain filter techniques have become the main methods in high-resolution SAR imaging. The traditional mean-value and median filters can smooth speckle noise efficiently. But they are non-adaptive [25] and the speckle noise is multiplicative [26], so the edge information is usually lost. Subsequently, many local adaptive statistic filters based on multiplicative noise were developed, for example, the Lee filter [27], the Kuan filter [28], the Frost filter [29], the enhanced Lee filter [30] and the enhanced Frost filter [31], the Gamma Map filter and the enhanced Map filter [32]. These filters not only reduce speckle noise by adjusting the size of the filtering window, but also reduce the resolution of the filtering window at the same time and make image edges and linear objects blurry. Although some edge information is well preserved, speckle noise is not restrained fully. In recent years, the well-developed wavelet transform technique has been utilized to restrain speckle noise, which can generally preserve edge information [33].

It is very difficult for any filter method to obtain optimal effect of both edge information saving and noise smoothing while restraining SAR image speckle noise. Therewith, in terms of practical application requirement, we propose data fusion filter method. Because the filtering algorithm based on space-domain can smooth speckle noise efficiently, while they blur edges and detailed information; wavelet filter based on wavelet transform may preferably preserve edge information, while the smoothing effect is not satisfactory. Therefore, we propose using wavelet analysis technique to fuse two or more single filter method for restraining speckle noise. This method can preserve edge, detailed and texture information well when it restrains speckle noise.

Assume that $A(i,j)$ is the SAR image data that has been filtered with space domain method, $B(i,j)$ is the SAR image data that has been filtered with wavelet transform method and $F(i,j)$ is the corresponding fusion image data, and (i,j) is the position of a pixel

in an image. The steps and principles of data fusion are as follows

(1) Choose wavelet function and two images that are filtered by single different filter method, and then match the two images.
(2) Decompose two images with wavelet analysis until the M layer, respectively.
(3) Fuse data of every decomposed layer, respectively. Because space domain filter may reduce the influence of speckle noise, the low frequency coefficient of the fused image directly adopts the low frequency coefficient of the filtered result with space domain filter, namely, $C_{M,F} = C_{M,A}$. But for high frequency part, it will adopt the weight index fusion method. Assume that $R(m,n)$ expresses the fused window whose size is $m \times n$, and I_A, I_B, σ_A^2, σ_B^2 is the mean and the variance of the pixel in window, respectively. The definitions of the weight factor α and β are given by

$$\begin{cases} \alpha = \sigma_A^2/(\sigma_A^2 + \sigma_B^2) \\ \beta = \sigma_B^2/(\sigma_A^2 + \sigma_B^2) \end{cases} \tag{30}$$

and the fusion formula is given by

$$R_{ij,F} = \alpha \times R_{ij,A} + \beta \times R_{ij,B}, \tag{31}$$

where R_{ij} is the data of center pixel in the window. According to Eq. (31), three high frequency coefficients of some layers are fused, respectively. Then the mentioned course will be repeated until the whole data of all decomposed floors is fused.
(4) Do wavelet reverse transform for the fused image data, then get the fused image $F(i,j)$.

4.3. Coherence-based smoothing speckle noise

The coherence of radar signal is the key technique for SAR improving resolution. At the same time, because of coherence, speckle noise comes into being. Accordingly, speckle noise can be smoothed through coherent principle. So we propose the coherent filter concept and corresponding filter method. The flow diagram of coherent filter algorithm is shown in Fig. 9.

It can be seen from the scattering characteristic of man-made objects and natural scene that the man-made objects have very strong coherence within large angle matching range, but natural scene can not form strong coherence unless sub-pixel level registration. Therefore, if SAR images are processed by the coherence, the coherence of speckle noise is not as strong as the man-made objects. If original SAR image subtracts from coherent SAR image, speckle noise may be smoothed, especially, uniformity region. Judging from statistical characteristic, coherent filter not only has good Edge Saved Index (ESI), but also has high equivalent number of looks (ENL). ENL is an index to weigh relative intensity of an image, which has how much speckle noise. It reflects the capability for a filter to restrain

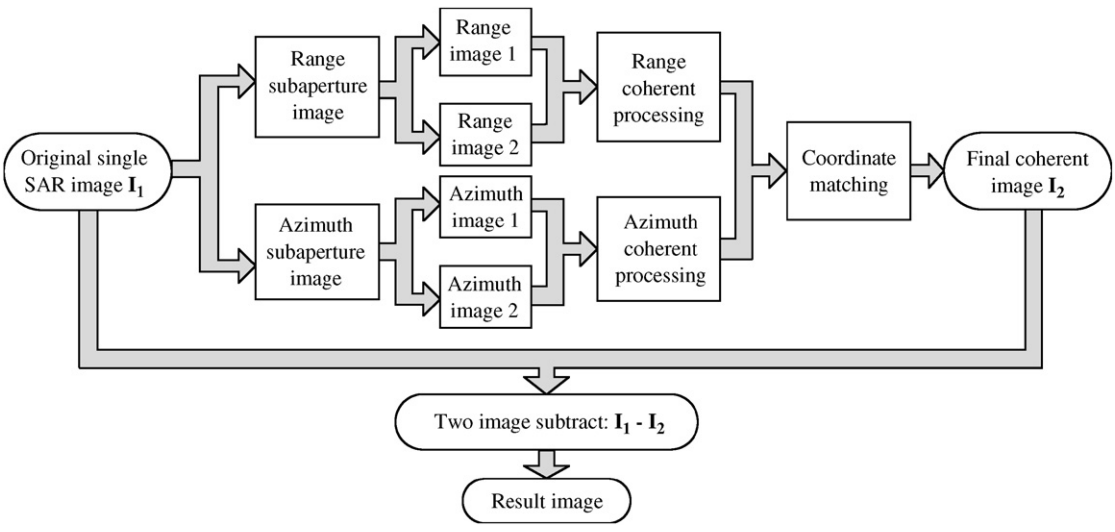

Fig. 9. The principle diagram of coherent filter for SAR image.

speckle noise. If ENL is higher, speckle noise is weaker in the image and the interpretation is better. The definition of ENL is given by

$$\mathrm{ENL} = I^2/\sigma^2, \tag{32}$$

where I and σ^2 are the mean and the variance of an image, respectively. ESI shows the edge-preserved capability for a filter to process an image. And it is classified into two types, which are horizontal ESI and vertical ESI. The higher the ESI is, the better the edge preserved capability is. The formula is given by

$$\mathrm{ESI} = \frac{\sum_{i=1}^{m} |\mathrm{DN}_{\mathrm{filter}R1} - \mathrm{DN}_{\mathrm{filter}R2}|}{\sum_{i=1}^{m} |\mathrm{DN}_{\mathrm{orginal}R1} - \mathrm{DN}_{\mathrm{orginale}R2}|}, \tag{33}$$

where, m is the number of the pixel, $\mathrm{DN}_{\mathrm{filter}R1}$ and $\mathrm{DN}_{\mathrm{filter}R2}$ or $\mathrm{DN}_{\mathrm{orginal}R1}$ and $\mathrm{DN}_{\mathrm{orginal}R2}$ are the gray values of left–right or up–down neighbor pixel at the edge connection along the filtered image or the original image, respectively.

In processing process, because of original SAR image subtracting from coherent SAR image, some object information is taken out, and they should be restored. The coherent image makes threshold processing, then it does non-coherent vector sum with the coherent image and the moved information restore. The filtered results with single algorithm and data fusion method are shown in Fig. 10, respectively. The filtered results with coherent filtering Algorithm for different scenes are shown in Fig. 11.

5. Uncertainty caused by object aspect angle (pose) sensitivity

Since what radar image reflects is the back-scattering coefficient of ground target, when the location, the structure, surface morphology and dielectric constant of the ground target are different, the tone and texture of an image will be different correspondingly. There are some factors, such as electromagnetic wavelength, incidence angle, ground object roughness, complex dielectric constant and angle reflector, which will make back-scattering coefficient produce uncertainty. In general, the higher the complex dielectric constant, the stronger the action of reflecting radar beam, and the smaller the penetration action. Complex dielectric constant shows a linear variation relative with the liquid water content of a unit volume [34]. When the liquid water content is low, the radar beam penetrating power is large and the reflected energy is small. When liquid water content is very high, the penetrating power will greatly decrease, and the reflected energy will increase. Therefore, with different liquid-water content of ground target, it is easy to generate the phenomenon of same thing different spectra or different thing same spectra. In practical SAR images, such as calm surface, airport runway, tiled road and flat roof, they are dark easily take up the phenomenon of different thing but same spectra. In the same way, the angle reflector shows

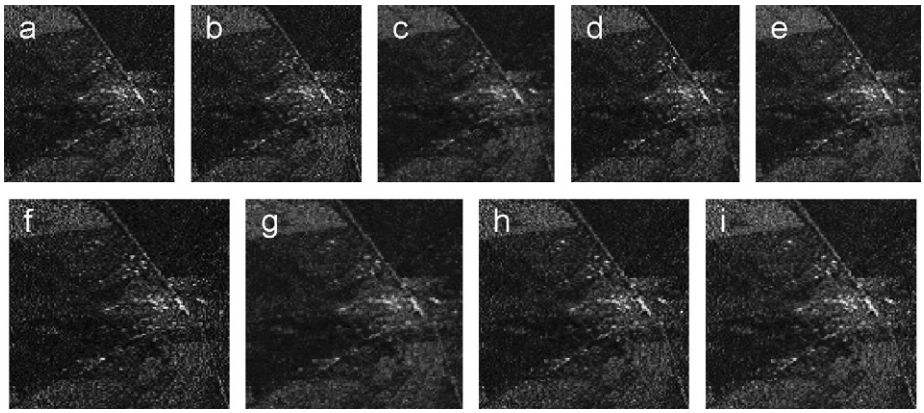

Fig. 10. Filter results comparison of SAR images. (a). single channels SAR image; (b) multi-look SAR image; (c) SAR image with mean filter; (d) SAR image with enhanced Frost filter; (e) SAR image with enhanced MAP filter; (f) SAR image with wavelet analysis filter, (g) SAR image with fusion filter to wavelet and mean; (h) SAR image with fusion filter of wavelet and EnFrost; and (i) SAR image with fusion filter of wavelet and EnMAP.

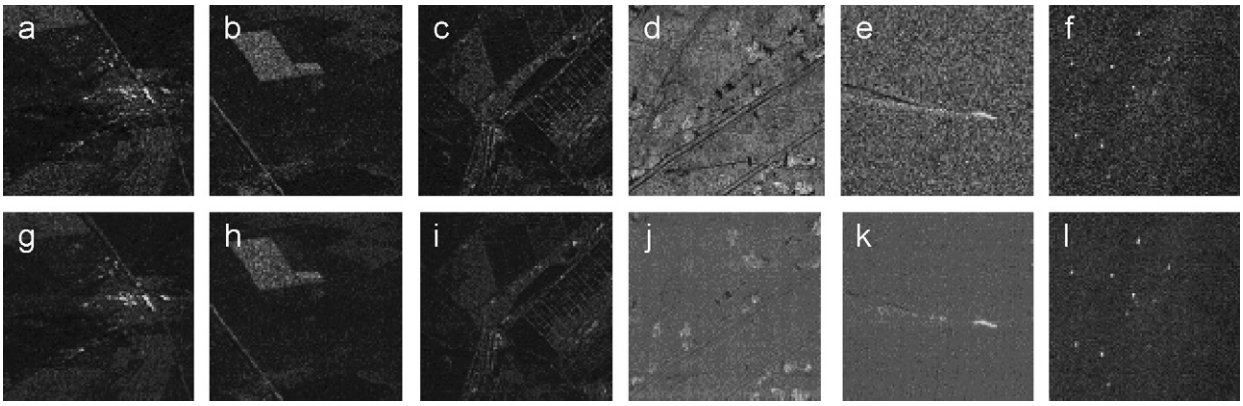

Fig. 11. The filtered results for different SAR images with coherent filtering algorithm, (a)–(f) original SAR images, (g)–(l) corresponding filtered SAR images, (a)–(d) flat and agricultural land, (e)–(f) ocean region, image size all 512×512.

bright point in SAR images, which is easy to be regarded as metal ground target. Majority tactical targets, like tank, vehicle, cannon, ship, airplane, missile, etc., and industrial establishments, such as high-tension power line tower, oil well, isolated small building, present as point targets in SAR image, which gives a lot of uncertainty for target recognition and classification.

An obvious difference between SAR images and optics images is that SAR images are especially sensitive to object azimuth angle. With different azimuth angles of an object, we can get different SAR images. It brings a great deal of matters and difficulties for target recognition and target classification, especially, target change detection and damage evaluation. Sometimes the target does not change at all, but its azimuth happens to change, which lead to different SAR image.

In high frequency field, the total backscattering of a radar target can be approximatively taken for the corresponding sum of all scattering centers [35]. These scattering centers provide abundant target information for us and they can be acted as good recognition reference in automatic target recognition (ATR). Therefore, we found the 2-D scattering center parameter model for SAR targets and extracted scattering center numbers to judge whether the target changes, as it provided some thoughts and methods for ascertaining uncertainty that is caused by target aspect angle.

According to the geometric theory of diffraction (GTD), if the wavelength of the incident excitation is small relative to the object extent, the backscattered field from an object consists of contributions from electrically isolated scattering centers. The backscattered field of an individual scattering center is described as a function of frequency f and aspect angle ϕ, and the total scattered field from a target is modeled as the sum of these individual scatterers [36–40]:

$$E(f,\phi;\theta)=\sum_{i=1}^{n}E_i(f,\phi;\theta_i), \tag{34}$$

where $\theta^{\mathrm{T}}=[\theta_1^{\mathrm{T}},\ldots,\theta_n^{\mathrm{T}}]$ and

$$E_i(f,\phi;\theta_i)=A_i\left(\mathrm{j}\frac{f}{f_c}\right)^{\alpha_i}\times\exp\left\{-\mathrm{j}\frac{4\pi f}{c}(x_i\cos\phi+y_i\sin\phi)\right\}. \tag{35}$$

Here, f is frequency, f_c is the radar center frequency, ϕ is aspect angle, and $c=3\times10^8\,m/\mathrm{s}$ is the propagation velocity. Each term $E_i(f,\phi;\theta_i)$ represents a single scattering center. The parameters x_i and y_i are the downrange and crossrange locations, A_i is the scattering center amplitude, and $\alpha_i\in[-1,-0.5,0,0.5,1]$ describes the frequency dependence. For multiple polarizations, A_i is a vector whose length is the number of polarization measurements available.

Eq. (35) does not consider the depending relation of scattering intensity of scattering center and illumination angle ϕ. If considering the relation, in terms of different scattering features that scattering represents along azimuth angle change, the scattering centers are classified into two types, which are localized scattering centers and distributed scattering centers. The localized scattering centers have localization echo in SAR images, including trihedrion, point object and sphere etc, and the

corresponding scattering is trihedral angle scattering, corner diffraction and edge diffraction. The scattering intensity can be expressed with decaying exponential function as follows:

$$S_i(f,\phi) = A_i \exp(-2\pi f \eta_i \sin\phi), \tag{36}$$

where η_i expresses the slight dependence of the scattering of localized scattering centers to azimuth. The distributed scattering centers usually contain some pixel units, such as dihedral scattering, flat plate specula, cylinder side and side edge diffraction. In accordance with physical optics (PO) method, all dependence relations of these scattering to azimuth have sinc function format, and it is

$$S_i(f,\phi) = A_i \operatorname{sinc}\left(\frac{2\pi f}{c} L_i \sin(\phi - \bar{\phi}_i)\right), \tag{37}$$

where L_i is the length of the scattering center, $\bar{\phi}_i$ is the orientation angle. In terms of Eqs. (34)–(37), the 2-D scattering center model of SAR target is given by

$$\begin{aligned} E(f,\phi,\theta) = \sum_{i=1}^{n} & A_i \left(\mathrm{j}\frac{f}{f_c}\right)^{\alpha_i} \\ & \times \exp\left[-\mathrm{j}\frac{4\pi f}{c}(x_i \cos\phi + y_i \sin\phi)\right] \\ & \times \exp(-2\pi f \eta_i \sin\phi) \\ & \times \operatorname{sinc}\left[\frac{2\pi f}{c} L_i \sin(\phi - \bar{\phi}_i)\right]. \end{aligned} \tag{38}$$

Eq. (38) may be written as

$$\begin{aligned} E(f,\phi,\theta) = \sum_{i=1}^{n} & A_i \left(\mathrm{j}\frac{f}{f_c}\right)^{\alpha_i} \\ & \times \exp[-\mathrm{j}2k(x_i \cos\phi + y_i \sin\phi)] \\ & \times \exp(-kc\eta_i \sin\phi) \\ & \times \operatorname{sinc}[kL_i \sin(\phi - \bar{\phi}_i)], \end{aligned} \tag{39}$$

where k is space wave number, and $k = 2\pi/\lambda$. From the Eq. (39), we may see that the main parameters are α and L, which include the geometric structure information of scattering center. α describes the geometric type of scattering center, and L describes the corresponding scattering center length. When they are combined, they can describe different basic type scattering structure more accurately and in detail and can supply more abundant target structure information for ATR. For localized scattering center, it still has parameter η_i, which describes the minute dependence relation of despondence and azimuth. For localized scattering centers, $L_i = \overline{\phi}_i = 0$ and $\eta_i \neq 0$; for distributed scattering centers, $\eta_I = 0$ and $L_i > 0$.

The parameters α and L in the model distinguish among several scattering geometries. The length L determines whether the scattering center is localized or distributed, while the frequency dependence relates to the curvature of the primitive scattering. If $\alpha = 1$, it is fiat surface scattering; if $\alpha = 1/2$, it is singly curved surfaces; if $\alpha = 0$, it is doubly curved surfaces. Table 1 shows some canonical scattering shapes which are corresponding the parameters α,L and η.

The set $(A_i, \alpha_i, x_i, y_i, \eta_i, L_i)$ of every scattering center parameter can be estimated by Eq. (39). In other words, the description of every scattering center will be obtained. The combination of each scattering center geometric description can infer the geometry shape of scattering object. When the number of scattering center is more, the parameter estimation dimension is the higher, and the burden of computation is large. But neural network may be used to resolve the computation burden and recognize the scattering center.

Table 1
Discrimination of canonical scattering shapes from α, L and η parameters values

α	L	η	Geometric structure of scattering body
1	$L>0$	$\eta=0$	Dihedral angel or flat scattering
	$L=0$	$\eta\neq0$	Trihedral angle scattering
1/2	$L>0$	$\eta=0$	Cylinder scattering
	$L=0$	$\eta\neq0$	The top of hat scattering
0	$L>0$	$\eta=0$	Doubly curved surface or straight edge specula scattering
	$L=0$	$\eta\neq0$	Sphere or point scattering
−1/2	$L>0$	$\eta\neq0$	Edge diffraction
−1	$L>0$	$\eta\neq0$	Corner diffraction
<−1	$L>0$	$\eta=0$	Cavity body or wave conductor

6. Conclusions

The uncertainty of SAR imaging causes many difficulties for the interpretation, judgment, recognition and classification of SAR images, so we must pay more attention to the influence caused by the uncertainty in SAR images and their applications. In order to reduce the uncertainty and improve the SAR images quality, we should research new imaging models, imaging algorithms and SAR image filtering methods, and discuss new and efficient approaches for SAR target recognition. Beginning with the principle SAR imaging, this paper discusses the influence of uncertainty for SAR imaging from several aspects, including Doppler parameter estimations, range migration correction, speckle noise filter and object aspect angle sensitivity and propose some methods or algorithms to improve these uncertainties. These methods have some theoretic and practical significance for studying SAR imaging and application further. On the further work, we will research the uncertainty and improvement from the system parameters and ground object parameters for SAR imaging.

Acknowledgments

The authors would like to thank the anonymous reviewers and editor for their careful reading. Their comments and suggestions have helped us to improve the clarity of the paper.

References

[1] J.C. Cheng, H.D. Guo, W.Z. Shi, et al., Uncertainty Problem of Remote Sensing Data, Science Publishing House, Beijing, China, 2004.
[2] Y. Ge, J.F. Wang, Y. Leung, Z.S. Wang, Uncertainty visualization of SAR Imaging system and application, Chin. Geo-information Sci. 3 (117) (2003) 86–90.
[3] Y.C. Bo, Research of Uncertainty and Scale Effect Brought From Remote Sensing Information, Chinese Science Academy, Beijing, China, 2002.
[4] D.M. Huo, Research of Uncertainty Processing and Evaluation Method for Remote Sensing Image Classification, Wuhan University, Wuhan, China, 2003.
[5] R.G. Congalton, K. Green, Assessing the Accuracy of Remotely Sensed Data: Principles and Practices, Lewis Publishers, 1999.
[6] S.W. Hu, H. Xu, Z.Z. Yu, Z.F. Pan, Discussion blurry uncertainty of remote sensing data, Mine Surv. of China (4) (2004) 19–21.
[7] J. R. Bennett, I. G. Cumming, R. A. Deane, The digital processing of seasat synthetic aperture radar data, in: IEEE International Radar Conference 1980. pp. 168–175.
[8] R.K. Raney, H. Runge, R. Bamler, et al., Precision SAR processing using chirp scaling, IEEE Trans. Geosci. Remote Sensing 32 (7) (1994) 786–799.
[9] R. Bamler, A comparison of Rang-Doppler and wavenumber SAR focusing algorithms, IEEE Trans. Geosci. Remote Sensing 30 (4) (1992) 706–713.
[10] S.Q. Huang, Research of Imaging Technology on Missileborne Slant Synthetic Aperture Radar, Xi'an Research Institute of Hi-Tech, Xi'an, China, 2004.
[11] T.S. David. SAR Image Formation: ERS SAR processor coded in MATLAB. 〈http://www.topex.ucsd.edu/insar/sar_image_formation.pdf.〉.
[12] S.N. Madsen, Estimating the Doppler centroid of SAR data, IEEE Trans. Aerosp. Electron. Syst. 25 (2) (1989) 134–140.
[13] Y.H. Huang, Imaging Processing and Motion Compensate of Spaceborne Synthetic Aperture Radar, Beijing University of Aeronautics and Astronautics, China, 1992.
[14] F.K. Li, D.N. Held, J. Curlander, C. Wu, Doppler parameter estimation for spaceborne synthetic aperture radars, IEEE Trans. Geosci. Remote Sensing 23 (1) (1985) 47–56.
[15] D. Blacknell, R.G. White, J.W. Wood, The prediction of geometric distortions in airborne SAR imagery from autofocus measurements, IEEE Trans. Geosci. Remote Sensing 25 (6) (1987) 775–781.
[16] M.C. Terry, Subaperture autofocus for synthetic aperture radar, IEEE Trans. Aerosp. Electron. Syst. 30 (2) (1994) 613–621.
[17] Y. T. Liu, et al., Radar Imaging Technique, Ha'erbin Industry University Publishing House, Ha'erbin, China, 2001.
[18] J. C. Curlander, C. Wu, A. Pang, Automatic preprocessing of spaceborne SAR data, in: Proceedings of the International Conference on Advanced Structural Steels, Japan, 2002, pp. 31–36.
[19] Y. P. Cheng, Study of several problems in SAR imaging, Xidian University Doctor Degree Paper, Xi'an, China, 2000.
[20] J. Moreira, A New method of aircraft motion error extraction from radar raw data for real time motion compensation, IEEE Trans. Geosci. Remote Sensing 28 (7) (1990) 620–626.
[21] J. Dall, A new frequency domain auto focus algorithm for SAR, in: Proceedings of International Geoscience and Remote Sensing Symposium, Helsinki, 1991, pp. 1069–1072.
[22] X. K. Yuan, Introduce to the Spaceborne Synthetic Aperture Radar, Defence Industry Publishing House Beijing, 2003.
[23] J.W. Goodman, Some fundamental properties of speckle, J. Opt. Soc. 66 (11) (1976) 1145–1150.
[24] F.T. Ulaby, F. Kouyate, B. Brisco, T.H. Lee Williams, Textural information in SAR images, IEEE Trans. Geosci. Remote Sensing 24 (2) (1986) 235–245.
[25] J.S. Lee, I. Jurkevich, Speckle filtering of synthetic aperture radar images: a review, Remote Sensing Rev. (8) (1994) 313–340.
[26] J.S. Lee, Speckle analysis and smoothing of synthetic radar images, Comput. Graphics Image Process. (17) (1981) 24–32.
[27] J.S. Lee, Digital image enhancement and noise filtering by use of local statistics, IEEE Trans. Pattern Anal. Mach. Intel. 2 (2) (1980) 165–168.
[28] D.T. Kuan, A.A. Sawchuk, T.C. Strand, P. Chavell, Adaptive noise smoothing filter for images with signal-dependent noise, IEEE Trans. Pattern Anal. Machine Intell. 7 (2) (1985) 165–177.

[29] V.S. Frost, J.A. Stiles, K.S. Shanmugan, J.C. Holtzman, A model for radar images and its application to adaptive digital filtering of multiplicative noise, IEEE Trans. Pattern Anal. Mach. Intell, 4 (2) (1982) 157–166.
[30] Z. B. Shi, K. Fung, A comparison of digital speckle filters, in: Proceedings of International Geoscience and Remote Sensing Symposium, 1994, pp. 2129–2133.
[31] A. Lopes, R. Touzi, E. Nezry, Adaptive speckle filters and scene heterogeneity, IEEE Trans. Geosci. Remote Sensing 28 (6) (1990) 992–1000.
[32] D.T. Kuan, A.A. Sawchuk, T.C. Strand, P. Chavel, Adaptive restoration of images with speckle, IEEE Trans. Acoust. Speech Signal Process. 35 (3) (1987) 373–383.
[33] D. D. Giusto, SAR image filtering using wavelet transform, in: Proceedings of International Geoscience and Remote Sensing Symposium, 1995, pp. 2153–2155.
[34] N. Shu, Microwave Remote Sensing Theory, Wuhan University Publishing House, Wuhan, China, 2003.
[35] M.J. Gerry, L.C. Potter, I.J. Gupta, et al., A parametric model for synthetic aperture radar measurements, IEEE Trans. Antennas Propag. 40 (7) (1999) 1179–1188.
[36] L.C. Potter, D.M. Chiang, R. Carriere, M.J. Gerry, A GTD-based parametric model for radar scattering, IEE Proc. Radar Sonar Navig. 6 (3) (1995) 58–67.
[37] D.F. Fuller, A.J. Terzuoli, P.J. Collins, R. Williams, Approach to object classification using dispersive scattering centers. IEE Proc. Radar,, Sonar Navig 15 (2) (2004) 85–90.
[38] A. Yeliz, L.M. Randolph, A scattering center model for SAR imagery, SPIE 3869 (1999) 76–85.
[39] A.K. Michael, L.M. Randolph, Feature extraction using attributed scattering center models on SAR imagery, SPIE 3721 (1999) 104–115.
[40] S.Q. Huang, D.Z. Liu, et al., Model and recognition of 2D scattering center for SAR target, Dyn. Continuous Discrete Impulsive Syst. Ser. B—Appl. Algorithms 13 (Part 2 S. I.) (2006) 639–642.